THE JOURNAL OF BIOLOGICAL CHEMISTRY VOL. 286, NO. 35, pp. 30911–30925, September 2, 2011

Lipid Raft Endocytosis and Exosomal Transport Facilitate Extracellular Trafficking of Annexin A2*[S]

Received for publication, June 12, 2011, and in revised form, July 5, 2011 Published, JBC Papers in Press, July 7, 2011, DOI 10.1074/jbc.M111.271155

Mallika Valapala[‡] and Jamboor K. Vishwanatha[‡§¶1]

From the [‡]Departments of Biomedical Sciences, [§]Molecular Biology and Immunology, and [¶]Institute for Cancer Research, University of North Texas Health Science Center, Fort Worth, Texas 76107

Annexin A2 (AnxA2), a Ca^{2+}-dependent phospholipid-binding protein, is known to associate with the plasma membrane and the endosomal system. Within the plasma membrane, AnxA2 associates in a Ca^{2+}dependent manner with cholesterol-rich lipid raft microdomains. Here, we show that the association of AnxA2 with the lipid rafts is influenced not only by intracellular levels of Ca^{2+} but also by N-terminal phosphorylation at tyrosine 23. Binding of AnxA2 to the lipid rafts is followed by the transport along the endocytic pathway to be associated with the intralumenal vesicles of the multivesicular endosomes. AnxA2-containing multivesicular endosomes fuse directly with the plasma membrane resulting in the release of the intralumenal vesicles into the extracellular environment, which facilitates the exogenous transfer of AnxA2 from one cell to another. Treatment with Ca^{2+} ionophore triggers the association of AnxA2 with the specialized microdomains in the exosomal membrane that possess raft-like characteristics. Phosphorylation at Tyr-23 is also important for the localization of AnxA2 to the exosomal membranes. These results suggest that AnxA2 is trafficked from the plasma membrane rafts and is selectively incorporated into the lumenal membranes of the endosomes to escape the endosomal degradation pathway. The Ca^{2+}-dependent exosomal transport constitutes a novel pathway of extracellular transport of AnxA2.

AnxA2[2] is a member of the multigene family of Ca^{2+} and phospholipid-binding proteins, which interact with negatively charged phospholipids in a Ca^{2+}-dependent manner (1). Plasma membrane-associated AnxA2 is implicated in several membrane-related events including fibrinolysis, exocytosis and endocytosis, cell-cell adhesion, and membrane-cytoskeletal interactions (2). AnxA2 is a soluble protein predominantly distributed in the cytosol of the cells at resting Ca^{2+} levels and translocated to cellular membranes under elevated concentrations of intracellular Ca^{2+}(3). *In vitro* studies using artificial membranes have shown that AnxA2 preferentially binds to the acidic phospholipids, which are enriched in the cytoplasmic leaflet of cellular membranes (4).

The mechanism of cell surface translocation of AnxA2 may occur via a non-classical secretory pathway as AnxA2 lacks a signal sequence that could direct it across the classical endoplasmic reticulum-Golgi secretory pathway (5). One of the central questions in understanding the Ca^{2+}-dependent plasma membrane dynamics of AnxA2 is how the protein is recruited from the intracytoplasmic leaflet of the plasma membrane to the extracytoplasmic leaflet to be localized to the cell surface.

Membrane association of AnxA2 is largely attributed to the hypervariable N-terminal domain that precedes the conserved Ca^{2+} binding core domain (6). Previous reports suggest that AnxA2 preferentially binds to cholesterol and phosphatidylinositol 4,5-bisphosphate-rich domains of the membrane called lipid rafts (7). Although AnxA2 influences the raft dynamics and promotes the formation of lipid microdomains, the mechanisms that influence the raft association and the subsequent functions of lipid raft-associated AnxA2 are not well understood.

Lipid rafts are implicated in diverse cellular processes including cell adhesion, membrane trafficking, and signal transduction events (8). The highly fluid raft microdomains serve as platforms for the segregation and sorting of proteins to different cellular compartments (9, 10). The most intriguing observation, however, is the involvement of lipid rafts in sorting of lipid and proteins in the endocytic and secretory pathways (11). Lipid raft endocytosis is characterized as a general mechanism for pathogen entry (12), recycling of extracellular ligands (13), and cell surface trafficking of glycosylphosphatidylinositol-anchored proteins (14). Recent studies have suggested that lipid raft-associated proteins are trafficked through the endocytic pathway as a result of invagination of the plasma membrane rafts into the endocytic vesicles (15). Proteins that are targeted to the endosomal pathway after internalization from the plasma membrane are progressively shuttled first to the early endosomes and later incorporated into the multivesicular endosomes (MVEs) or endosome carrier vesicles to be destined to the late endosomal pathway (16). MVEs are critical intermediates of the endocytic pathway that are formed when the limiting membrane of the early endosomes invaginates into its lumen (17). MVEs contain secreted intralumenal components called exosomes with protein and lipid composition identical to the

* This work was supported in part by National Center on Minority Health and Health Disparities Grant MD001633.

[S] The on-line version of this article (available at http://www.jbc.org) contains supplemental Figs. S1–S3.

[1] To whom correspondence should be addressed: 3500 Camp Bowie Blvd., Fort Worth, TX 76107. Fax: 817-735-0423; E-mail: Jamboor.vishwanatha@unthsc.edu.

[2] The abbreviations used are: AnxA2, annexin A2; MVE, multivesicular endosome; AnxA2WT-GFP, GFP-tagged to the C terminus of wild-type AnxA2; AnxA2Y23E-GFP and AnxA2Y23F-GFP, GFP-tagged to AnxA2Y23 phosphorylation mutants; TS, Triton-soluble fraction; TI, Triton-insoluble fraction; GM1, monosialotetrahexosylganglioside; GM3, NeuAcα 2,3Galβ1, 4Glc-ceramide or *N*-acetylneuraminylgalactosylceramide; CTXB, cholera toxin subunit B; N-Rh-PE, *N*-(lissamine rhodamine B sulfonyl)-phosphatidylethanolamine; DRM, detergent-resistant membranes; Tfr, transferrin receptor; MOC, Manders's overlap coefficient; MβCD, methyl-β-cyclodextrin.

endosomes reflecting their endosomal origin (18). Exosomes not only possess proteins that are necessary for their biogenesis and maintenance but also contain several plasma membrane and cytosolic proteins (19). Exosomes are also identified to possess distinct membrane domains enriched in cholesterol and GM1 gangliosides and similar in composition to the plasma membrane rafts (20, 21). The presence of raft-like domains in the exosomes suggests that exosomes participate in the sorting of raft-associated proteins. Raft-like domains are found to be present not only in the MVE intralumenal vesicles but also in the late endosomes, and they are thought to originate by the endocytosis of the plasma membrane rafts occurring via clathrin-dependent (22) and -independent pathways (15).

In the present study we questioned whether AnxA2 is trafficked from the plasma membrane lipid rafts to the intralumenal vesicles of the MVEs to be later released into the extracellular space upon fusion of the MVEs with the plasma membrane. We first sought to determine the molecular mechanisms by which AnxA2 is initially recruited to the plasma membrane lipid rafts. Upon elevation of cytosolic Ca^{2+} levels, AnxA2 is sorted from the plasma membrane rafts first to the exosomal membranes. Within the exosomal membrane, AnxA2 is localized to distinct regions that possess raft-like characteristics, and exosomes are also identified to serve as potential intercellular carriers of AnxA2.

The data presented here provide novel insights into the membrane dynamics of AnxA2. We suggest the importance of Tyr-23 phosphorylation in the Ca^{2+}-dependent recruitment of AnxA2 to the plasma membrane rafts. Localization of AnxA2 in the lipid rafts targets AnxA2 into the intralumenal vesicles of the MVE and its further assortment into the raft-like regions of the exosomal membrane. Upon fusion of the MVEs with the plasma membrane, the MVE intralumenal vesicles, called exosomes, are secreted into the extracellular space, and the released AnxA2 rebinds to the surface of the target cell in a Ca^{2+}-dependent manner.

EXPERIMENTAL PROCEDURES

Antibodies and Reagents

The following antibodies were used: mouse monoclonal anti-AnxA2 (BD Biosciences), mouse monoclonal anti-Na^+,K^+-ATPase (a6-FC) (Developmental Studies Hybridoma Bank (University of Iowa), rabbit polyclonal anti-PGK (25), rabbit polyclonal anti-GFP (D5.1) (Cell Signaling), mouse monoclonal anti-GFP (Roche Diagnostics), mouse monoclonal anti-phosphotyrosine (Tyr(P)-100) (Cell Signaling), mouse monoclonal anti-caveolin 1 (pY14) (BD Biosciences), mouse monoclonal anti-transferrin receptor (H68.4) (Zymed Laboratories Inc.), mouse monoclonal anti-heat shock cognate protein-70 (SPA-816) (hSC-70) (Stressgen), rabbit polyclonal anti-CD44 antibody (Abcam), rabbit polyclonal anti-CD81 (H-121) (Santa Cruz Biotechnology), anti-Rab5 antibody (Cell signaling). Anti-mouse and anti-rabbit IgG (Sigma) and peroxidase-conjugated goat anti-rabbit and anti-mouse IgG were from Promega. Reagents were purchased from the following sources: Ca^{2+} ionophore A23187, methyl-β-cyclodextrin (Sigma), filipin (Sigma), Alexa-conjugated cholera toxin subunit B (CTXB) (Invitrogen), sulfo-NHS-Biotin (Pierce), avidin-conjugated Sepharose (Sigma), Fluo-3 AM (Invitrogen), phosphatidyl(*N*-sulforhodamine B sulfonyl)ethanolamine (N-Rh-PE) (Avanti Polar Lipids), brefeldin A (Sigma), Triton X-100 (Sigma), CHAPS (Sigma), BODIPY-Laccer (Avanti Polar lipids), Alexa594-conjugated transferrin (Molecular Probes).

Cell Culture and Ionophore Treatment

NIH 3T3 mouse fibroblasts and MDA-MB231 cells were cultured at 5% CO_2 in Dulbecco's modified Eagle's medium high glucose and low glucose medium respectively (DMEM; Invitrogen) supplemented with 10% fetal bovine serum (FBS) and 5% penicillin-streptomycin. A polyclonal population of LNCaP-C1 cells stably expressing GFP was cultured in RPMI 1640 medium (Invitrogen) supplemented with 10% FBS and 5% penicillin-streptomycin. For ionophore treatment, subconfluent cultures were treated with 5 μM Ca^{2+} ionophore A23187 for the indicated periods of time. For transfections, cells were cultured in 100-mm dishes to 70% confluence. 20 μg of DNA was incubated with 30 μl of Lipofectamine 2000 (Invitrogen) and was later added to 15 ml of Opti-MEM (Invitrogen) for 6 h and returned to normal growth medium.

Plasmids and Constructs

For the construction of a plasmid expressing full-length AnxA2, the cDNA of AnxA2 was cloned into the pEGFP-N1 vector. The N-terminal phosphomimetic and non-phosphomimetic mutants at Tyr-23 were generated by using QuikChange site-directed mutagenesis kit (Stratagene). In this report, the plasmids are referred to as AnxA2WT-GFP, AnxA2Y23E-GFP, and AnxA2Y23F-GFP.

Confocal Microscopy

For immunocytochemistry, cells expressing AnxA2Y23E-GFP and AnxA2Y23F-GFP were treated with 5 μM Ca^{2+} ionophore A23187. The cells were later subjected to monosialoganglioside GM1 labeling with 8 μg/ml Alexa 555-conjugated cholera toxin B subunit. The cells were washed, fixed with 4% paraformaldehyde, and subjected to immunocytochemistry. The coverslips were mounted on glass slides with Prolong Gold mounting media (Invitrogen). Confocal images were obtained using Zeiss LSM 510 META confocal microscope equipped with a 63× Plan-Apochromat objective and HeNe1, HeNe2, and argon lasers. The weighted colocalization coefficients were calculated using the Zeiss LSM enhanced colocalization software (Zeiss), which is a measure of the sum of the number of co-localizing pixels relative to the sum of the total number of pixel intensities after background correction.

EDTA Elution and Cell Surface Biotinylation

Confluent cultures were washed with 0.5 mM EDTA and PBS buffer (Versene, Invitrogen) for 20 min at 37 °C, and the supernatant was designated EDTA eluate. Cell surface proteins were subjected to biotinylation with 0.5 mg/ml sulfo-NHS biotin (Pierce) and recovered with avidin-conjugated Sepharose (Sigma) as previously described with slight modifications (63). Briefly, cells were washed with ice-cold PBS, chilled on ice for 5 min to block endocytosis, and biotinylated with 1 mg of EZ-

Link Sulfo-NHS-LC-Biotin (Pierce) for 1 h at 4 °C. Cells were later washed twice with ice-cold PBS and subsequently incubated on ice with 50 mM glycine, PBS for 15 min to quench the biotinylation reaction. Subsequently, cells were lysed in TNE buffer (25 mM Tris-HCl, pH 7.5, 150 mM NaCl, 5 mM EDTA) containing 1% Triton X-100 plus protease and phosphatase inhibitor mixture (Promega). The post-nuclear supernatants were incubated in 60 μl of NeutrAvidin beads (Pierce). After incubation for 1 h at 4 °C, the supernatant was removed, and the beads were washed twice with each buffer A (10 mM Tris-Cl, pH 7.4, 150 mM NaCl, 2 mM EDTA, 0.2% Nonidet P-40), boiled in sample buffer, and subjected to SDS-PAGE Western immunoblot analysis. Alternatively, the post-nuclear supernatants were recovered and subjected to Triton X-100 extraction of the detergent-resistant membranes (DRMs) as described below.

Isolation of Exosomes

Fetal bovine serum contains endogenous exosomes; to eliminate exosomes from FBS, the culture medium (DMEM, 10% FBS, and 5% penicillin-streptomycin) was centrifuged overnight at 120,000 × *g*. Exosomes were isolated from the culture medium by serial centrifugation as previously published (64). The culture medium was subjected to serial centrifugations at 800 × *g* for 10 min to remove the cells and at 12,000 × *g* for 30 min to remove the cell debris. The exosomes were pelleted from the supernatant by centrifugation at 100,000 × *g* for 15 h, washed, resuspended, and repelleted in PBS using a SW28 rotor (Beckman).

Extraction of Lipid Rafts by Triton X-100

Separation of the membrane into Triton-soluble and -insoluble components was performed as published (35). Briefly, cells were lysed in buffer A (25 mM MES, 150 mM NaCl, pH 6.5). The lysate was treated with an equal volume of the buffer A mixed with 2% Triton X-100, 2 mM Na_3VO_4, and 2 mM PMSF and incubated on ice for 30 min. The lysates were centrifuged at 14,000 × *g* for 30 min, and the supernatant was collected and referred to as the Triton-soluble (TS) fraction. The insoluble pellets were resuspended with buffer B (1% Triton X-100, 10 mM Tris-Cl, pH 7.6, 500 mM NaCl, 2 mM Na_3VO_4, 60 mM β-octylglucoside, and 1 mM PMSF) for 30 min on ice and centrifuged at 14,000 × *g* for 20 min. The supernatant was collected and referred to as the Triton-insoluble (TI) fraction.

Sucrose Gradient Fractionation

Cells—Lipid raft fractions were isolated according to the previously published protocols with a few modifications (32). Briefly cells were grown to near confluence, transfected, and treated in four 100-mm dishes. The cells were lysed in 500 mM Na_2CO_3, pH 11, with a mixture of protease and phosphatase inhibitors, and the lysate was homogenized with 20 strokes in a prechilled Dounce homogenizer followed by homogenization with a Polytron homogenizer 3 times for 10 s with intervals of 10–15 s followed by sonication 3 times for 20 s with an interval of 60 s. Two ml of the homogenized sample was mixed with 2 ml of 90% sucrose in MBS (25 mM MES, 150 mM NaCl, pH 6.0). A discontinuous sucrose gradient was generated by overlaying with 4 ml of 35% sucrose in 1× MBS and 250 mM Na_2CO_3 followed by overlaying with 4 ml of 5% sucrose in 1× MBS and 250 mM Na_2CO_3. The gradient was centrifuged at 40,000 × *g* in a SW40Ti rotor (Beckman). Twelve 1-ml fractions were collected from the top of the tube, and the fractions were subjected to trichloroacetic acid (TCA) precipitation followed by SDS-PAGE and Western immunoblotting.

Exosomes—Exosomes collected by serial centrifugation were subjected to further purification as described previously (20). The exosomal pellet was resuspended in 5 ml of 2.6 M sucrose, 20 mM Tris-HCl, pH 7.2, a linear sucrose gradient of (2.0 – 0.25 M sucrose, 20 mM Tris-HCl, pH 7.2) was layered on the top of the exosome suspension in a SW41 tube for 16 h at 270,000 × *g* (Beckman), and the pellets were subjected to SDS-PAGE and Western immunoblotting.

Lipid rafts were isolated from the exosomes as described (21). Freshly isolated vesicles (2 mg) from the culture medium were suspended in 1.5 ml of buffer A (50 mM Tris·HCl, pH 7.2/150 mM NaCl, pH 7.2) in combination with 1% Triton X-100 or 1% CHAPS with protease and phosphatase inhibitors. The suspension was mixed in 1.5 ml of 95% sucrose, overlaid with 3 ml of 35% sucrose and 3 ml of 5% sucrose, and centrifuged at 150,000 × *g* for 16 h at 4 °C. 1-ml fractions from the top were collected and subjected to SDS-PAGE and immunoblot analysis.

Fluorescent Lipid N-Rh-PE Labeling of the MVEs and Intracellular Ca^{2+} Labeling with Fluo-3 AM

MVEs were labeled with N-Rh-PE as described previously (30). Briefly the ethanolic solution of the fluorescent lipid (<1% v/v) was injected by a Hamilton syringe into the medium, and after vigorous vortexing the cells were incubated in the medium for 60 min at 4 °C. The cells were later washed with PBS to remove any unbound lipids and loaded with 15 μM Fluo-3 AM (Molecular Probes) for 30 min at 37 °C. After subjecting the cells to ionophore treatment, cells were washed with PBS and immediately mounted on glass coverslips and visualized under the Zeiss LSM 510 confocal microscope using a 40× objective.

Immunofluorescence Analysis of Exosomal Protein Transfer

Exosomes were freshly harvested from the culture medium of MDA-MB231 cells, suspended in 1× PBS, and quantified for protein concentration by a BCA assay (Pierce). LNCaP-C1 cells were cultured on coverslips and incubated with 30 μg of exosomes collected from MDA-MB231 cells for 12 h at 37 °C. The cells were fixed and stained with anti-AnxA2 antibody (1:1000). LNCaP-C1 cells were incubated in 0.5 mM EDTA for 1 h to chelate off MDA-MB231-derived cell surface AnxA2.

Quantification of Released Exosomes

Quantification of secreted exosomes was performed by measuring the activity of acetylcholine esterase as previously described (27). Briefly, 50 μl of the pelted exosomes was suspended in 100 μl of PBS, 37.5 μl of this PBS-diluted fraction was incubated in the presence of 1.25 mM acetylthiocholine and 0.1 mM 5′m5′-dithiobis(2-nitrobenzoic acid), and the reaction mixture was brought to a final volume of 300 μl in a 96-well plate. The incubation was carried out at 37 °C, and the change in absorbance at 412 nm was monitored every 5 min. The data

presented represent the enzymatic activity 20 min after incubation.

Electron Microscopy

Enriched exosomal fractions were fixed for 10 min at room temperature in 2% formaldehyde in PBS, pH 7.4, and either adsorbed onto freshly ionized Formvar/carbon-coated grids for 20 min or filtered onto 1-cm, 0.45-mm cellulose nitrate filter paper circles. Some grids were negatively stained in 2% uranyl acetate in water. Other grids and filters were washed in PBS containing 0.01 M glycine and subsequently processed like coverslips as described. Briefly, after blocking in PBS supplemented with 10% FCS, the grids/filters were incubated in primary IgG (20 μg/ml) in 10% FCS (4 h to overnight), washed in PBS containing 0.01 M glycine and 2.5% FCS, and incubated in the secondary goat anti-rabbit 5-nm gold conjugate diluted 1:50 in 10% FCS (2 h). Filters were washed in PBS containing 5% FCS and 0.01 M glycine followed by 100 mM cacodylate buffer, pH 7.4, fixed in 1% OsO4 in 100 mM cacodylate buffer for 1 h at 4 °C, treated with1% tannic acid in 100 mM cacodylate buffer (pH 7.4), and subsequently stained en bloc in 2% uranyl acetate for 2 h. The filters were then dehydrated in ethanol, embedded in Epox, and processed for routine electron microscopy. Sections were picked up onto 300 mesh nickel grids and stained with lead citrate and uranyl acetate. Grids were observed in a Tecnai 12TWIN transmission electron microscope operating at 100 kV.

RESULTS

Phosphorylation at Tyr-23 Promotes the Association of AnxA2 with the Low Density TI Membrane Fractions on Ionophore Stimulation—Increase in the intracellular levels of Ca^{2+} is known to precede the activation of pp60c-Src, a tyrosine kinase that phosphorylates AnxA2 at Tyr-23 (26). We investigated the involvement of Tyr-23 phosphorylation in cell surface trafficking of AnxA2 on ionophore treatment. EDTA eluates from cells expressing AnxA2Y23E-GFP and stimulated with ionophore were immunoblotted with GFP antibody to reveal a marked increase in the cell surface levels of AnxA2Y23E-GFP as compared with the vehicle control (Fig. 1*A*, *left panel*). However, in cells expressing AnxA2Y23F-GFP, both basal and ionophore-stimulated cell surface levels of AnxA2 were markedly reduced (Fig. 1*A*, *right panel*). Ionophore treatment did not result in any significant changes in the intracellular levels of AnxA2 in cells expressing either of the constructs. PGK and Coomassie staining of the gel were used as loading controls for whole cell lysates and EDTA eluates, respectively.

Immunoprecipitation of EDTA eluates from cells expressing AnxA2WT-GFP with anti-GFP (Fig. 1*B*) and anti-AnxA2 antibodies (supplemental Fig. 1*A*) revealed a marked increase in the cell surface levels of tyrosine-phosphorylated AnxA2. The role of tyrosine phosphorylation in the cell surface translocation of AnxA2 was further confirmed by pretreating the cells with sodium orthovanadate, a tyrosine phosphatase inhibitor, before stimulation with ionophore. For recovery of cell surface proteins we used biotinylation and avidin-based affinity purification. We observed an increase in the ionophore-induced cell surface levels of AnxA2 in cells pretreated with sodium orthovanadate, indicating that augmentation of tyrosine phosphorylation increases the association of AnxA2 to the cell surface (supplemental Fig. 1*B*). These results demonstrate that in addition to intracellular Ca^{2+}, phosphorylation at Tyr-23 regulates the trafficking and association of AnxA2 with the plasma membrane. To investigate the role of Tyr-23 phosphorylation in the association of AnxA2 with the lipid raft domains of the plasma membrane, we separated the plasma membrane into raft and non-raft regions based on their solubility in Triton X-100. Immunoblotting with the non-raft marker, transferrin receptor (Tfr), raft marker caveolin-1, and cytosolic PGK was performed to ascertain the purity of the TS non-raft, low density TI raft, and cytosolic fractions, respectively. Ionophore treatment resulted in increased association of AnxA2Y23E-GFP with the TI raft fractions, which is accompanied by a concomitant increase in the cell surface levels of AnxA2 compared with the cells treated with the DMSO control (Fig. 1*C*). An increase in the association of AnxA2Y23E-GFP with the TS non-raft fractions was also observed upon ionophore treatment. The association of AnxA2Y23F-GFP with the TI and TS fractions was markedly reduced in ionophore-stimulated cells, and a decrease in the cell surface expression of AnxA2 was also evident in both the ionophore and DMSO-treated cells (Fig. 1*D*).

To further demonstrate the importance of Tyr-23 phosphorylation in the raft association of AnxA2, cells transfected with AnxA2Y23E-GFP or AnxA2Y23F-GFP were either unstimulated or stimulated with the ionophore. The lipid rafts were subsequently labeled with Alexa 594-conjugated CTXB, which preferentially binds to GM1 gangliosides of the raft microdomains. Immunostaining for CTXB and GFP indicated a predominant colocalization of AnxA2Y23E-GFP with the GM1-rich raft microdomains, which was markedly reduced in the cells expressing AnxA2Y23F-GFP on ionophore treatment (Fig. 2*C*, *right panel*). In cells not treated with the ionophore, the extent of lipid raft formation was moderate, and both proteins, AnxA2Y23E-GFP and AnxA2Y23F-GFP, were retained in the cytosol (Fig. 1*E*).

Colocalization analysis was performed using WCIF_imageJ colocalization analysis tool. The extent of colocalization was measured by calculating the Pearson's correlation coefficient (PCC), which is used to measure the correlation of intensity distribution between the two channels (red and green), and Manders's overlap coefficient (MOC) indicates the actual overlap of two signals. Because MOC is a true representation of colocalization, we have estimated the extent of colocalization by measuring the MOC. The MOC values for the cells expressing AnxA2Y23E-GFP and AnxA2Y23F-GFP in the presence of the ionophore was measured to be 0.82 ± 0.03 and 0.25 ± 0.05, respectively. These results suggest a significant colocalization of Tyr-23-phosphorylated AnxA2 in the raft domains compared with the non-phosphorylated AnxA2.

Immunoprecipitation of TS and TI fractions from cells expressing AnxA2Y23E-GFP, AnxA2Y23F-GFP, and empty GFP vector indicated an increased recovery of AnxA2-GFP in the TI fractions of cells expressing AnxA2Y23E-GFP compared with the cells expressing AnxA2Y23F-GFP (supplemental Fig. 1*C*). Triton extraction of the cells expressing the empty GFP vector

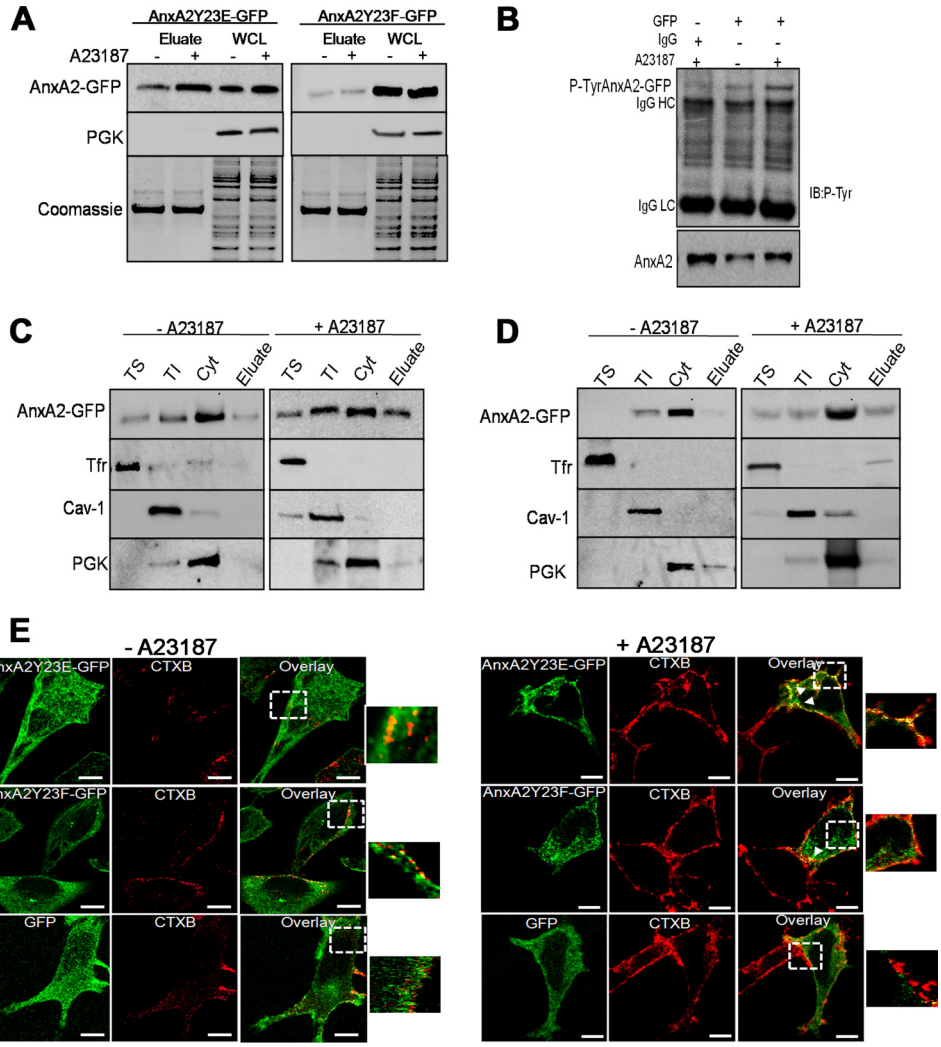

FIGURE 1. **Tyrosine 23 phosphorylation is essential for Ca^{2+}-dependent association of AnxA2 to the TI fractions.** *A*, GFP immunoblotting of EDTA eluates and whole cell lysates (*WCL*) isolated from cells expressing AnxA2Y23E-GFP and AnxA2Y23F-GFP in the presence and absence of ionophore is shown. PGK and Coomassie staining were used as loading controls for WCL and EDTA eluates, respectively. *B*, EDTA eluates from AnxA2WT-GFP-expressing cells were immunoprecipitated with anti-GFP antibody and immunoblotted (*IB*) with phosphotyrosine antibody. The endogenous levels of AnxA2 are shown in the *lower panels*. *IgGHC*, IgG heavy chain; *IgGLC*, IgG light chain. *C* and *D*, cells transfected with AnxA2Y23E-GFP and AnxA2Y23F-GFP were treated with either the ionophore or DMSO control. The vehicle control and ionophore-treated cells were incubated in EDTA and PBS buffer to collect the EDTA eluates, and after lysis, the cytosolic fraction (*Cyt*) was separated, and the plasma membrane was subjected to fractionation with Triton X-100 into TS and TI fractions. The purity of the fractions was determined by immunoblotting with caveolin (*Cav-1*), Tfr, and PGK antibodies. The distribution of AnxA2 in each of the fractions was analyzed by immunoblotting with AnxA2 antibody. *E*, ionophore-stimulated cells (*right panel*) and vehicle control-treated cells (*left panel*) expressing AnxA2Y23E-GFP and AnxA2Y23F-GFP were incubated with CTXB (*red*) and subjected to immunocytochemistry with GFP antibody (*green*). *Bars*, 20 μm.

followed by immunoprecipitation of the TS and TI extracts from AnxA2Y23E-GFP-transfected cells with control IgG provided negative controls.

We further tested if tyrosine-phosphorylated AnxA2 could be immunoprecipitated from the raft microdomains on ionophore treatment. For this purpose immunoprecipitation with GFP antibody was performed on TI extracts collected from ionophore stimulated and unstimulated cells. Tyrosine-phosphorylated AnxA2 was observed in the TI fractions of cells stimulated with the ionophore (supplemental Fig. 1*D*). The endogenous levels of AnxA2 in the input fractions are shown in the supplemental Fig. 1*D lower panel*. These results show that the association of AnxA2 with the detergent-resistant raft domains of the plasma membrane is dependent on the phosphorylation status of AnxA2 at Tyr-23.

Tyrosine 23 Phosphorylation Imparts on AnxA2 the Ability to Associate with Low Buoyant Density Lipid Rafts Isolated on Sucrose Floatation Gradients—To confirm the importance of Tyr-23 phosphorylation in the raft association of AnxA2, we separated the raft microdomains based on their density on sucrose flotation gradients. The cholesterol-rich light membrane fractions 4–6 were distributed at the interface between 5 and 35% and contain an enrichment of raft marker caveolin-1; the heavier membrane fractions 7–9 showed a predominant expression of the non-raft marker Tfr; most cellular cytosolic proteins were localized to the bottom of the gradient to fractions 10–12. In ionophore-unstimulated cells, AnxA2 was found to be predominantly localized to the heavier fractions with very little distribution in the high and low density fractions of the membrane, reflecting the principal distribution of the

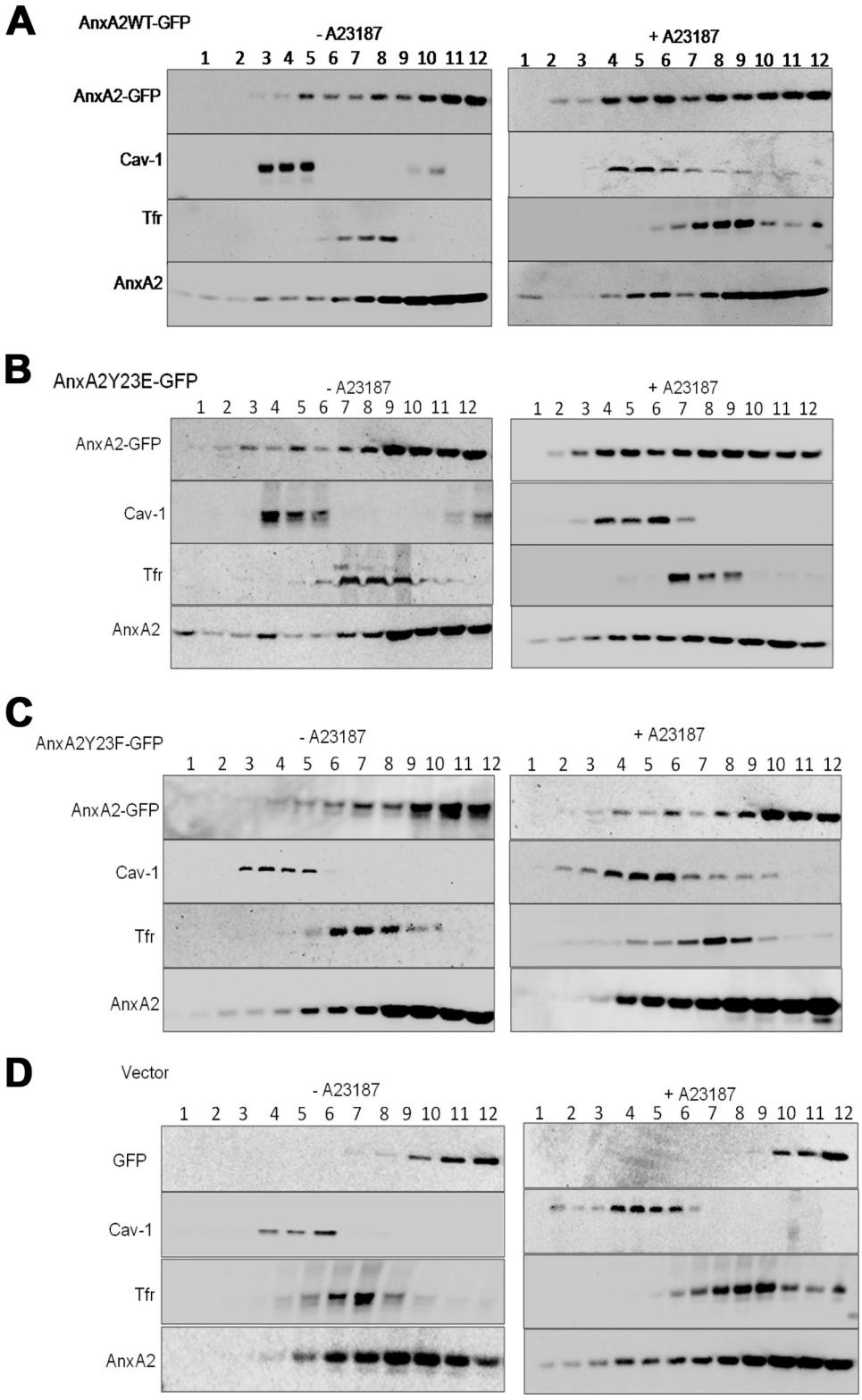

FIGURE 2. **AnxA2 is recruited to the low density sucrose flotation gradients on ionophore stimulation.** *A*, resting and stimulated NIH 3T3 cells transfected with AnxA2WT-GFP were lysed in Na_2CO_3 buffer and subjected to 45–5% discontinuous sucrose-density gradients. Twelve fractions were collected, and after TCA precipitation, they were subjected to Western immunoblot analysis with AnxA2 antibody to determine the distribution of AnxA2 in each of the fractions. Fractions were immunoblotted for caveolin-1 (*Cav-1*) and Tfr to identify the lighter raft and heavier non-raft regions of the membrane, respectively. *Fraction 1* represents the top of the gradient. *Fractions 4–6* represent the lighter fractions, and *fractions 7–12* represent the heavier fractions. *B* and *C*, the distribution of AnxA2 in the raft, non-raft, and the cytosolic fractions was determined in cells transfected with AnxA2Y23E-GFP and AnxA2Y23F-GFP and either stimulated or unstimulated with the ionophore. *D*, ionophore-treated and -untreated cells transfected with the empty vector pEGFP-N1 were fractionated on sucrose gradients. The amount of AnxA2 in each fraction was quantified by scanning three independent gels using the Alpha Imager software.

protein in the cytosol (Fig. 2, *A–C*, *left panels*). On ionophore stimulation, however, we observed a significant flotation of AnxA2 to the lighter sucrose fractions in cells expressing AnxA2WT-GFP and AnxA2Y23E-GFP (Fig. 2, *A* and *B*, *right panels*). In ionophore-treated cells expressing AnxA2Y23F-GFP, however, the association of the protein to the lighter fractions was significantly compromised, and the protein is predominantly localized to the heavier fractions (Fig. 2*C*, *right panel*). Cells transfected with empty GFP vector showed the localization of GFP to the cytosolic fractions in both unstimulated and ionophore-stimulated cells (Fig. 2*D*, *left* and *right panels*). In the above experiments, endogenous levels of AnxA2 showed increased association with the raft fractions in ionophore-stimulated cells compared with the unstimulated controls (Fig. 2, *A–D*). Densitometry analysis of the Western immunoblots revealed that ~30–40% of the total cellular protein was localized to the low density rafts in ionophore-stimulated cells transfected with AnxA2WT-GFP and AnxA2Y23E-GFP, respectively, as opposed to 5% association in cells transfected with AnxA2Y23F-GFP. These results also provide compelling evidence that phosphorylation of AnxA2 at Tyr-23 is critical for the Ca^{2+}-dependent raft association of AnxA2.

Depletion of Cellular Cholesterol Inhibits the Ca^{2+}-dependent Translocation of AnxA2 to the Low Density Triton-insoluble Regions of the Membrane—Because raft microdomains are involved in the sorting of proteins across the plasma membrane (14, 23), we examined the effect of depletion of membrane rafts on the extracellular trafficking of AnxA2. Methyl-β-cyclodextrin (MβCD) extracts cholesterol and induces variable amounts of cholesterol in the biological membranes, thereby disrupting the integrity of the lipid rafts. The effective concentration of MβCD required to deplete cholesterol from the cellular membranes of NIH 3T3 cells was determined from a previous study (24). Pretreatment of NIH 3T3 cells with MβCD solubilized a significant fraction of AnxA2 from the cell surface of ionophore-stimulated cells (Fig. 3*A*). MβCD-pretreated cells showed ~30% increase in cell surface levels of AnxA2 as compared with ~80% increase in untreated cells upon ionophore stimulation for 6 h.

Previous studies have indicated that AnxA2 is effectively released from the cholesterol-containing liposomes by treatment with filipin, a cholesterol-sequestering drug that inhibits lipid raft-dependent endocytosis (25). In our studies we observed that filipin inhibits the endocytosis of CTXB but does not influence the endocytosis of transferrin (supplemental Fig. 2). We studied the effect of filipin on the lipid raft localization and extracellular trafficking of AnxA2 in the presence of the ionophore. NIH 3T3 cells were incubated with filipin before treatment with the ionophore for the indicated periods of time, and extracellular AnxA2 was recovered by cell surface biotinylation. The cells were later processed for DRM isolation. Western immunoblot analysis of the cell surface and pooled DRM fractions indicated that ionophore treatment induces not only the cell surface expression of AnxA2 but also results in an increased association of AnxA2 with the DRM fractions. In addition, ionophore-induced extracellular and DRM association of AnxA2 was inhibited in cells pretreated with filipin (Fig. 3*B*). These results show that Ca^{2+}-dependent association of AnxA2 with the cell surface and the DRMs is largely dependent on the cellular levels of cholesterol. To determine the Ca^{2+}-dependent association of AnxA2 to the lipid rafts in the presence or absence of MβCD, we performed co-staining of AnxA2-GFP fusion proteins with CTXB, a marker frequently used to label lipid rafts. In ionophore-untreated cells AnxA2 was observed to be diffusely distributed in the cytosol and is scarcely localized to the CTXB-rich regions of the membrane (Fig. 3*C*, *top panel*). In the presence of MβCD, the CTXB-positive staining in the membrane was reduced, and AnxA2 remained predominantly in the cytosol (Fig. 3*C*, *second panel*). In cells treated with the ionophore, AnxA2WT-GFP co-localized with CTXB in the membrane and also in discrete compartments in the cytosol (Fig. 3*C*, *third panel*). A marked reduction in the CTXB and AnxA2-GFP colocalization in both the plasma membrane and internalized vesicles was observed when cells were pretreated with MβCD in the presence of the ionophore (Fig. 3*C*, *fourth panel*). We also observed that cytosolic AnxA2 co-localized with LAMP-1, a late endosomal marker in cells treated with the ionophore (Fig. 3*C*, *fifth panel*). LAMP-1 was also found to be co-localized with CTXB in the cytosol (Fig. 3*C*, *sixth panel*). Lack of colocalization of AnxA2WT-GFP with calnexin, an endoplasmic reticulum marker, further confirmed that these vesicles belong to the endosomal system (Fig. 3*C*, *seventh panel*). The extent of AnxA2 and CTXB colocalization at the membrane was measured to be 0.78 ± 0.0.06 in ionophore-treated cells. Upon treatment with MβCD before ionophore treatment, the MOC values for AnxA2 and CTXB colocalization was measured to be 0.29 ± 0.08.

AnxA2 Is a Component of the Secretory Exosomes Released from Ionophore-stimulated Cells—Previous studies have suggested that proteins that are trafficked to the intracellular lipid raft-containing vesicles are routed to the MVE pathway and lysosomes (8). We wanted to determine whether AnxA2 is a secretory component of the exosomes, which are the intralumenal vesicles of the MVEs. For this purpose we first investigated ionophore-induced formation of MVEs in NIH 3T3 cells. To visualize the ionophore-induced formation of intracellular MVEs, NIH 3T3 cells preloaded with a fluorescent lipid analog N-Rh-PE were simulated with ionophore. A significant increase in the number of N-Rh-PE-stained intracellular MVEs was observed around the perinuclear region in a time-dependent manner upon ionophore treatment (Fig. 4*A*). Intracellular MVEs typically enclose a number of small 30–100-nm intralumenal vesicles characterized as exosomes. To establish that ionophore-induced MVE formation is associated with increased secretion of exosomes, cells were treated with monensin, a drug that stimulates MVE exocytosis and enhances the secretion of exosomes, and wortmannin, a drug that inhibits the formation of MVEs. Quantification of secreted exosomes revealed a marked increase in the number of secreted exosomes in monensin and ionophore-treated cells compared with the wortmannin and untreated control cells (Fig. 4*B*). To provide further proof of the role of Ca^{2+} in influencing the secretion of exosomes, the cells were treated with either ionophore alone or ionophore in combination with either EDTA or BAPTA-AM. A significant increase in the number of secreted exosomes was observed in cells stimulated with ionophore alone compared

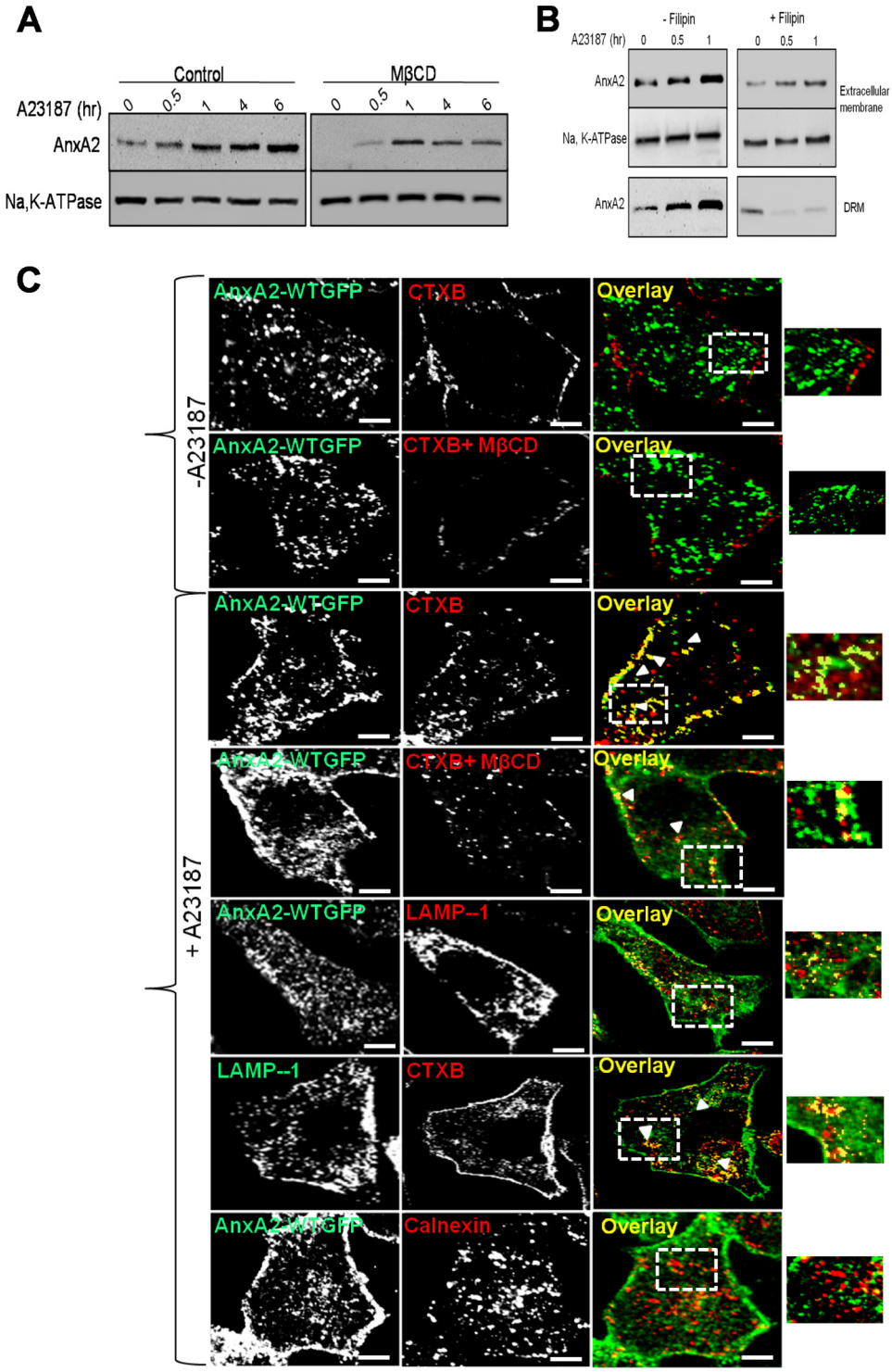

FIGURE 3. **Association of AnxA2 with cholesterol-rich regions of the membrane.** *A*, NIH 3T3 cells were treated with 5 mM MβCD for 20 min to deplete the cholesterol in the cellular membranes before treatment with 5 μM ionophore for the indicated periods of time. The cell surface-biotinylated extracts were subjected to immunoblot analysis for AnxA2, and the blots were reprobed for Na^+,K^+-ATPase for protein loading. *B*, NIH 3T3 cells pretreated with filipin were untreated or treated with the ionophore for the indicated periods of time (30 min and 1 h). Western immunoblotting of cell surface and DRM-associated AnxA2 recovered by cell surface biotinylation was followed by DRM extraction. *C*, confocal microscopy of NIH 3T3 fibroblasts expressing AnxA2WT-GFP untreated (*panels 1* and *2*) and treated with the ionophore (*panels 3–5*) is shown. Colocalization of AnxA2WT-GFP with CTXB in the presence or absence of MβCD (*panels 3* and *4*, respectively) and calnexin (*panel 5*). *Bars*, 20 μm.

with the cells stimulated with ionophore in combination with either EDTA or BAPTA-AM (Fig. 4*C*). We also observed that ionophore stimulation induced a marked increase in the number of secreted exosomes in a time-dependent manner in comparison to the unstimulated cells (Fig. 4*D*). To visualize the secretion of exosomes in a Ca^{2+}-dependent manner, cells were preloaded with Fluo-3 AM followed by labeling of the MVEs with a fluorescent lipid analog N-Rh-PE. The formation of

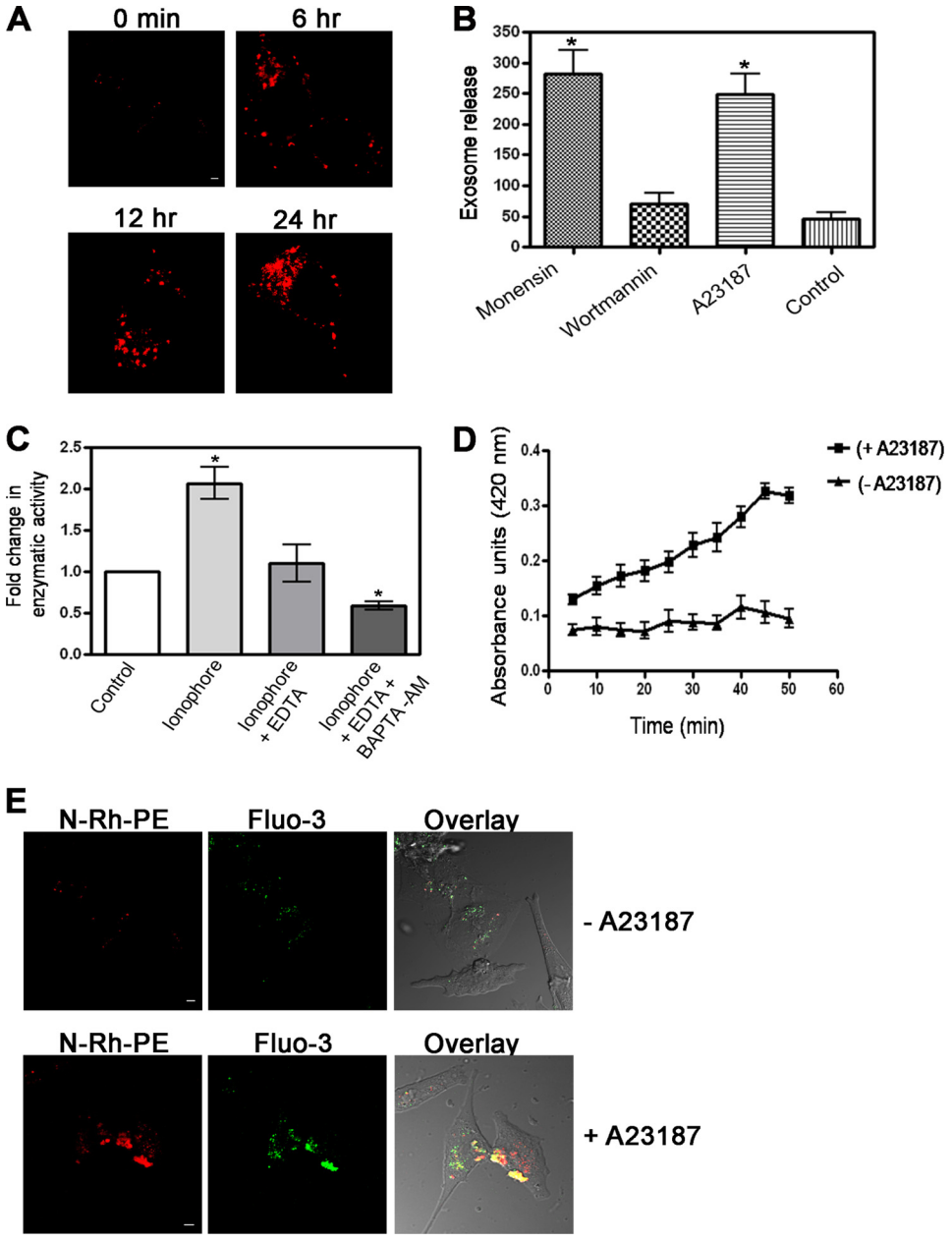

FIGURE 4. **Ionophore treatment induces the secretion of exosomes in NIH 3T3 cells.** *A*, confocal microscopy of NIH 3T3 cells preloaded with the fluorescent lipid analog N-Rh-PE and stimulated with the ionophore for the indicated periods of time are shown. *Bars*, 20 μm. *B*, shown is quantification of secreted exosomes over 24 h in untreated cells and cells treated with monensin (1 μM), wortmannin (50 nM), and A23187 (5 μM). *C*, exosomes collected from the culture medium of cells stimulated with ionophore in combination with 1.5 mM EDTA and 20 μM BAPTA-AM were quantitated by measuring the activity of acetylcholine esterase E (*AChE*). The -fold change in the enzymatic activity was plotted by normalizing the activity of the control to 1. * represents the significance at $p \leq 0.5$. *D*, quantification of the time-dependent secretion of the exosomes in the absence and presence of the ionophore by measuring the activity of acetylcholine esterase E is shown. The data are plotted as the mean absorbance units ± S.E. *versus* time in min. *E*, NIH 3T3 cells were preloaded for 1 h at 37 °C with 15 μM Fluo-3 AM, and the cells were later loaded with N-Rh-PE for 3 h at 37 °C and left untreated (*upper panels*) or treated (*lower panels*) with the ionophore. The colocalization of Fluo-3 AM and N-Rh-PE at dense areas closer to the plasma membrane indicates the presence of intracellular Ca^{2+} in the MVEs. *Bars*, 20 μm.

MVEs containing luminal Ca^{2+} was observed in ionophore-stimulated cells, which were markedly reduced in unstimulated cells (Fig. 4*E*). Taken together, these results further support that ionophore treatment induces the release of secreted exosomes.

Based on our observations that ionophore stimulation results in increased secretion of exosomes, we next determined whether AnxA2 is associated with secretory exosomes in a Ca^{2+}-dependent manner. Exosomes were extracted from the culture medium by serial centrifugation, and the recovered high speed pellet was further purified by layering on sucrose gradients. Exosomes are known to migrate to a density ranging from 1.06–1.15 g/ml in a linear sucrose gradient (33). Consistent with these observations, upon ionophore treatment, NIH 3T3-secreted exosomes migrated to fractions with a density of 1.08–1.16 g/ml and co-fractionated with hsc70 and Tfr (Fig. 5*A*). The purity of the exosomal fraction was further confirmed by immunoblotting the exosomes collected from the pooled sucrose gradient fractions and the cell lysate with antibodies against exosomal resident proteins and markers of the endoplasmic reticulum (calnexin) and mitochondrion (cytochrome

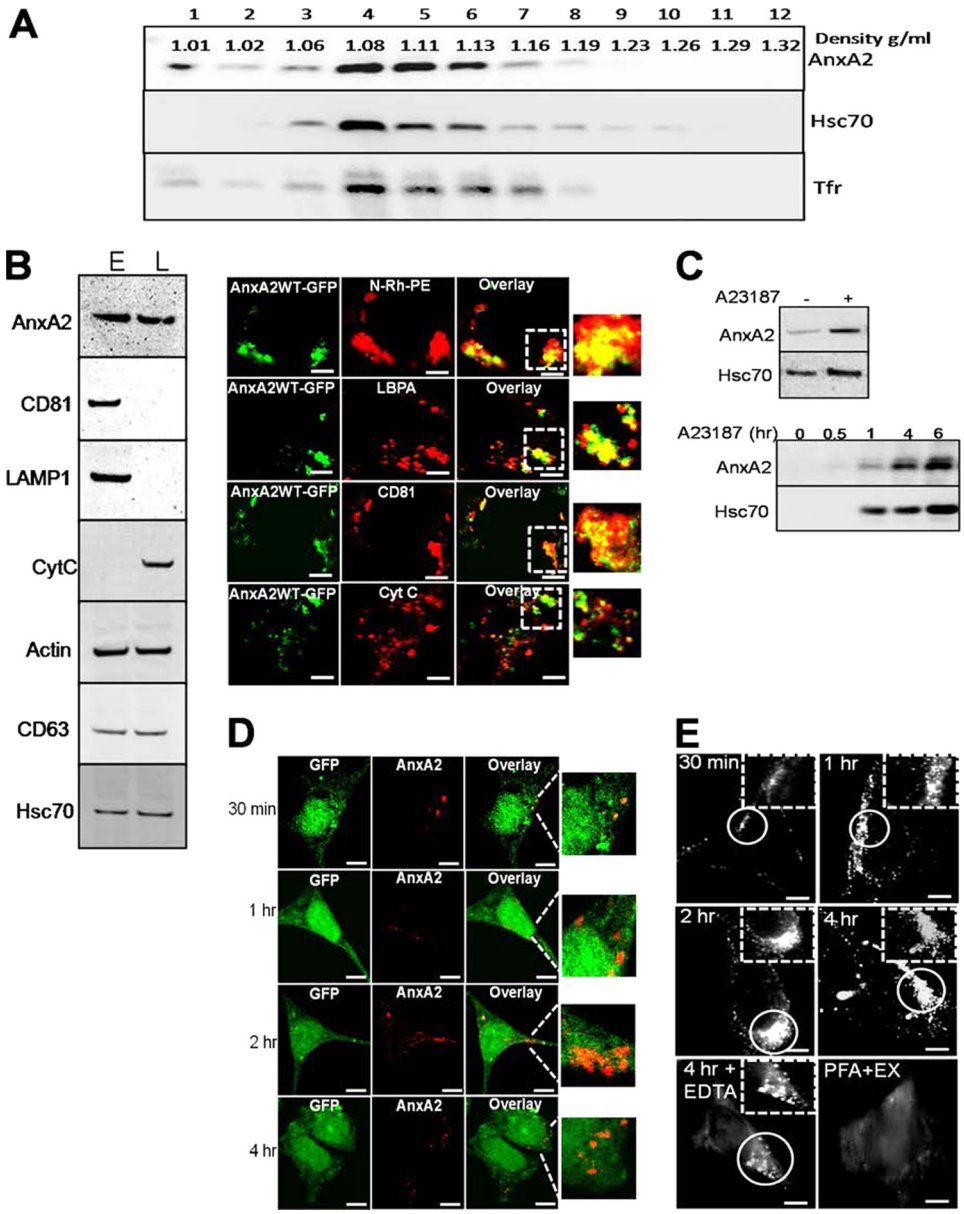

FIGURE 5. **Exosomal association of AnxA2 on ionophore stimulation.** *A*, pelleted exosomes were subjected to flotation on linear sucrose gradients (0.5–2 M sucrose) and subjected to ultracentrifugation. The fractions were collected and analyzed for expression of AnxA2 and exosome markers hsc70 and Tfr. Exosomes are shown to migrate to their characteristic density on the sucrose gradient. *B*, Western immunoblotting of the exosomal pellet and whole cell lysate with exosomal protein markers (CD81, CD63, hsc70, and LAMP-1), endoplasmic reticulum (*ER*), and mitochondrial (cytochrome *c* (*CytC*)) markers (*left panel*) is shown. Colocalization of intracellular MVEs expressing AnxA2WT-GFP with the fluorescent lipid analog (N-RH-PE), lysobisphosphatidic acid (*LBPA*), CD81 and cytochrome *c* (right panel). *Bars*, 20 μm. *L*, whole cell lysate; *E*, exosomal membrane. *C*, exosomes collected from ionophore-treated cells were subjected to Western immunoblot analysis to detect the expression of AnxA2 and hsc70 (*upper panel*). Exosomes were collected from cells stimulated with ionophore for the indicated periods of time and probed for AnxA2 and hsc70 (*lower panel*). *D*, LNCaP-C1 cells stably expressing empty GFP (*green*) were incubated with exosomes derived from MDA-MB231 cells for 30 min to 4 h. The overlay images indicate AnxA2-specific immunostaining on the surface of LNCaP-C1 cells (*left panel*). *E*, LNCaP-C1 were incubated with MDA-MB231-derived exosomes for the incubated periods of time and subjected to total internal reflection fluorescence microscopy. As a control, cells were treated with 2% paraformaldehyde (*PFA*) after incubation with exosomes (*EX*) and analyzed by total internal reflection fluorescence microscopy (*right panel*). *Bars*, 20 μm.

c). As shown in Fig. 5*B*, the expression of AnxA2 was observed in the exosomal pellet along with the expression of exosomal makers (CD81, LAMP-1, CD63, and hsc70). The absence of calnexin and cytochrome *c*, which are markers for the endoplasmic reticulum and mitochondria, further confirmed the purity of the exosomal pellet (Fig. 5*B*, *left panel*). To confirm the association of AnxA2 with the MVEs, we studied the distribution of GFP-tagged-AnxA2 and the exogenously delivered N-Rh-PE, which is sorted and retained in the MVEs. Within 6 h of transient transfection with AnxA2WT-GFP plasmid, the expression of AnxA2 was observed around the perinuclear region, which co-localized with N-Rh-PE (in 92% of the cells tested, $n = 47$). GFP-tagged AnxA2 co-localized with lysobisphosphatidic acid, a late endosomal marker (in 78% of the cells tested, $n = 53$), and CD81, an exosomal raft-enriched protein (in 83% of the cells tested, $n = 51$). AnxA2 did not co-localize with the mitochondrial marker cytochrome *c* (Fig. 5*B*, *right panel*). Next, we wanted to demonstrate the Ca^{2+}-dependent

association of AnxA2 with the exosomes. We observed that ionophore treatment resulted in increased exosomal levels of both AnxA2 and hsc70 (Fig. 5*C*, *upper panel*), suggesting the ionophore-induced secretion of the exosomes. Furthermore, we quantitated the extent of exosomal secretion after ionophore treatment. Exosomes collected from the ionophore-treated cells for the indicated periods of time showed increased levels of AnxA2, which are accompanied by a concomitant increase in the levels of a exosomal resident protein, hsc70 (Fig. 5*C*, *lower panel*).

To determine whether AnxA2 secreted from the exosomes can be exogenously transferred from one cell type to another cell type, we made use of AnxA2-null LNCaP-C1 cells stably expressing GFP and exosomes derived from MDA-MB231 cells. Cancer cells are known to secrete abundant levels of exosomes (34), and hence, we made use of a breast cancer cell line, MDA-MB231, for exogenous exosomal transfer. LNCaP-C1 cells were incubated with exosomes derived from MDA-MB231 cells for a period of 30 min to 4 h and subjected them to immunostaining with AnxA2 antibody. AnxA2-specific immunostaining was observed as punctate spots on the surface of LNCaP-C1 cells (Fig. 5*D*). Furthermore, incubation of LNCaP-C1 cells with MDA-MB231-derived exosomes for prolonged periods of time (4 h) resulted in the internalization of AnxA2 as visualized by the intracellular localization of AnxA2-specific immunostaining.

To further analyze incorporation of AnxA2 in LNCaP-C1 cells delivered from exogenous MDA-MB231-derived exosomes, we performed total internal reflection fluorescence microscopy to detect AnxA2-specific immunostaining in the subplasmalemmal regions and on the cell surface. Total internal reflection fluorescence microscopy showed an accumulation of AnxA2-positive exosomes on the cell periphery that was detectable as early as 30 min after incubation with exosomes. Incubation of exosomes for 4 h resulted in their subsequent internalization in the intracellular endosomal compartments. LNCaP-C1 cells incubated with exosomes for 4 h and treated with EDTA to chelate off peripheral AnxA2 showed the presence of only the internalized exosomes around the perinuclear regions. We observed that exosome internalization is an active process, as cross-linking the proteins with paraformaldehyde before the addition of exosomes prevented both exosome accumulation and intracellular entry (Fig. 5*E*).

AnxA2 Associates with the Low Density Triton-insoluble Regions of the Exosomes in Ionophore-stimulated Cells—We recovered the low density Triton-insoluble fractions from the exosomes and analyzed the distribution of AnxA2. Because NIH 3T3 cells secreted basal levels of exosomes under unstimulated conditions, it was not experimentally feasible to recover the low density Triton-insoluble membranes from these cells. Triton-permeated exosomal fractions from ionophore-stimulated cells were overlaid on sucrose gradients and immunoblotted for CD81 (exosomal raft-associated protein) and AnxA2. AnxA2 was found to be enriched in the low density fractions overlapping with CD81 (Fig. 6*A*). To address the role of Tyr-23 phosphorylation in the association of AnxA2 with exosomes on ionophore treatment, we collected the whole cell lysate, plasma membrane, and exosomal membrane fractions from cells expressing AnxA2WT-GFP, AnxA2Y23E-GFP, and AnxA2Y23F-GFP. The SDS-PAGE and immunoblotting with AnxA2 antibody revealed the distribution of AnxA2 in these fractions. As shown in Fig. 6*B*, ionophore treatment resulted in an increased association of both AnxA2WT-GFP and AnxA2Y23E-GFP with the plasma membrane and exosomal membrane as opposed to the markedly diminished distribution of AnxA2Y23F-GFP. Furthermore, to demonstrate the association of AnxA2 with the TI fractions of the exosomal membrane, the exosomal membranes from ionophore-stimulated cells were permeated with Triton X-100 and incubated in the presence of 1% CHAPS and layered on sucrose flotation gradients. Increased association of AnxA2-GFP fusion protein with the low density exosomal raft-like domains was observed in cells expressing AnxA2WT-GFP and AnxA2Y23E-GFP (Fig. 6, *C* and *D*, respectively). In contrast, cells expressing AnxA2Y23F-GFP showed a markedly diminished association of AnxA2 with the exosomal raft-like domains (Fig. 6*E*). The fractions were also immunoblotted with CD81 and Tfr to identify the low density and high density membrane fractions, respectively. To further demonstrate the association of wild-type AnxA2 and Tyr-23 phosphorylation mutants with the secreted exosomes, we performed flow cytometry analysis of exosomes. As shown in supplemental Fig. 3, the exosomes contained a strong expression of surface CD81 and CD63 compared with the isotype controls. In contrast, the expression of CD45 and Na^+,K^+-ATPase, which are plasma membrane markers, was not observed on the exosomes, confirming that the exosomal preparation was not contaminated by fragments of the plasma membrane. Moreover, the exosomes showed a strong expression of AnxA2WT-GFP and AnxA2Y23E-GFP in ionophore-stimulated cells. However, the expression of AnxA2Y23F-GFP was significantly compromised. When exosomes were depleted of Ca^{2+} by treating with EDTA, a marked reduction in the endogenous levels of AnxA2 was observed, suggesting that AnxA2 is bound to the surface of exosomes in a Ca^{2+}-dependent manner.

To further characterize the localization of AnxA2 in the secretory exosomes, we performed electron microscopy of the exosomes released from the conditioned medium of ionophore-treated and -untreated cells. Release of exosomes from the basal cells was observed to be significantly lower than cells treated with the ionophore. Immunogold labeling localized AnxA2 to small irregularly shaped vesicles with sizes ranging from 20 to 40 nm in basal cells. The exosomes released from basal cells (Fig. 6*F*, *left panel*) did not seem to possess a defined morphology, and the expression of AnxA2 was found to be predominantly in the lumen. Exosomes isolated from ionophore-treated cells, however, had a defined cup-like morphology with sizes ranging from ~100 to 150 nm. Immunoelectron micrographs also showed a predominant surface expression of AnxA2 in exosomes along with luminal expression of AnxA2 (Fig. 6*F*, *right panel*).

DISCUSSION

Our studies demonstrate that cell surface trafficking of AnxA2 is a multistep process mediated by a highly coordinated sequence of events in the intracellular endocytotic pathway. Elevated levels of Ca^{2+} mobilize cytosolic AnxA2 to the choles-

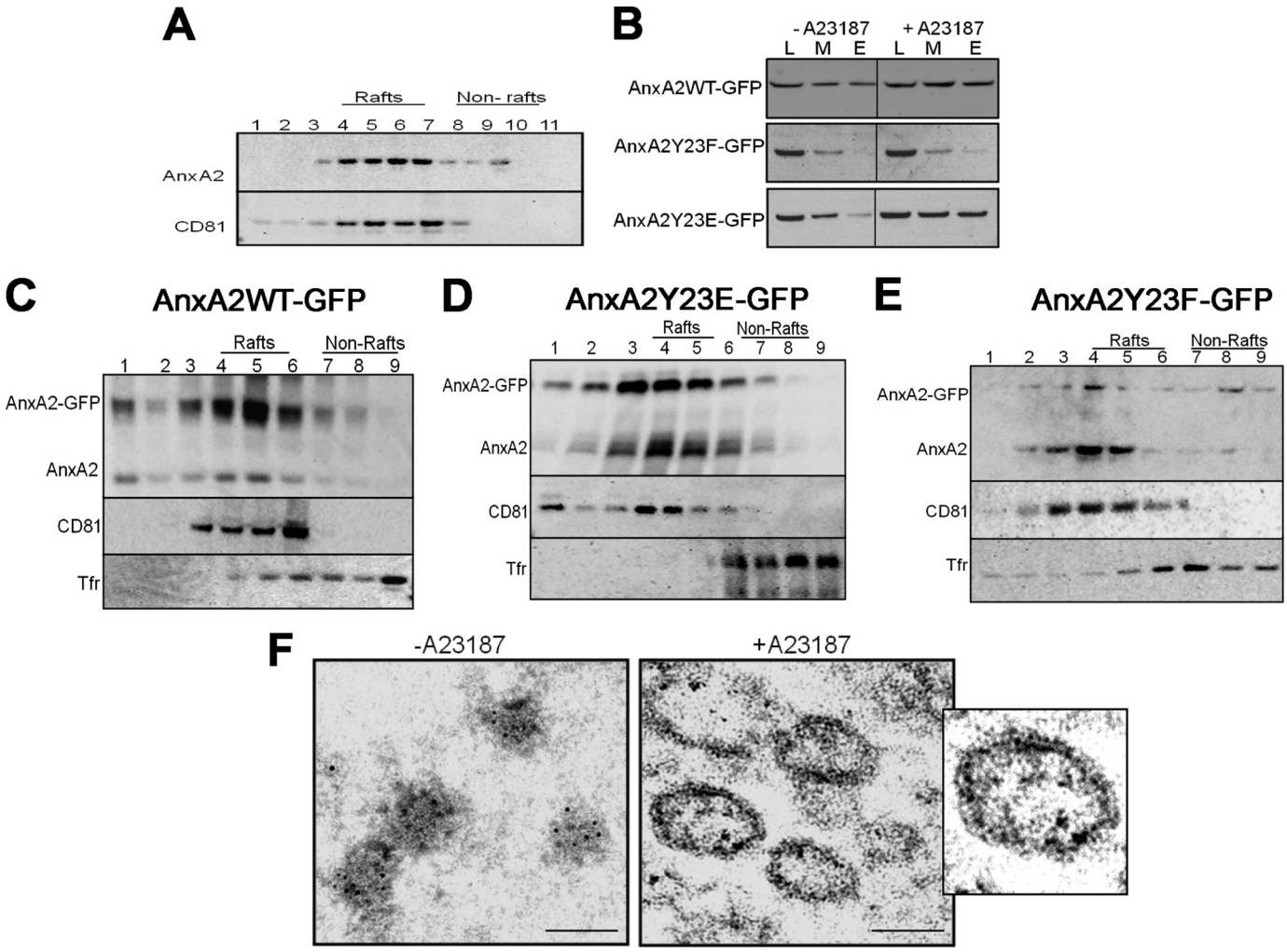

FIGURE 6. **Separation of exosomal membranes on sucrose flotation gradients.** *A*, the exosomal pellet from pooled sucrose flotation gradients was incubated in the presence of 1% CHAPS and 1% Triton X-100, respectively, and layered on sucrose gradients. The fractions were collected from the top and subjected to Western immunoblotting with anti-CD81 and anti-AnxA2 antibodies. *B*, equal amounts of protein from the whole cell lysate (*L*), plasma membrane (*M*), and exosomal (*E*) fractions collected from the ionophore-stimulated cells expressing AnxA2WT-GFP, AnxA2Y23E-GFP, and AnxA2Y23F-GFP were analyzed by Western immunoblot for the expression of AnxA2. *C*, *D*, and *E*, exosomal pellets from the above fractions recovered from cells expressing AnxA2WT-GFP, AnxA2Y23E-GFP, and AnxA2Y23F-GFP, respectively, were separated by differential centrifugation on sucrose gradients after incubation with 1% CHAPS. Fractions were immunoblotted with AnxA2 and probed for raft (CD81) and non-raft (Tfr) marker proteins. *F*, shown is electron microscopy of the secreted exosomes from ionophore-treated and -untreated cells on staining with immunogold-labeled AnxA2 antibody. Scale, 50 nm.

terol-enriched domains of the plasma membrane called lipid rafts. Phosphorylation at Tyr-23 imparts on AnxA2 its ability to bind and stabilize with the lipid raft microdomains. After recruitment to the plasma membrane lipid rafts, AnxA2 is internalized from the lipid rafts by caveolae-mediated endocytosis. We observed the Ca^{2+}-dependent association of AnxA2 in the raft-like regions of the MVE intralumenal vesicles. This process could be due to the endocytosis of plasma membrane lipid rafts by clathrin-dependent or independent pathways. Furthermore, AnxA2 associated with the MVE intralumenal vesicles is released into the extracellular space upon fusion of the MVEs with the plasma membrane. We also observed the association of AnxA2 in the raft-like regions of the secretory exosomes, which are originally the intralumenal vesicles of the MVE. Finally, our results indicate that the association of AnxA2 with the raft-like regions of the plasma membrane and the organelle membranes is largely dependent on the phosphorylation at Tyr-23.

One of the unresolved issues in AnxA2 biology is how the protein is translocated to the cell surface subsequent to stimuli that induce an increase in the intracellular levels of Ca^{2+}(2, 3). In an effort to identify the membrane dynamics that result in Ca^{2+}-dependent cell surface translocation of AnxA2, we used an ionophore-stimulated model in NIH 3T3 cells. Ionophore-induced elevation of intracellular Ca^{2+} has been a particularly valuable model to study Ca^{2+}-dependent relocation of AnxA2 to cellular membranes (36). Relocation to the plasma membrane is related to several functions of AnxA2 including membrane trafficking, signaling events associated with Ca^{2+} handling, and membrane-cytoskeletal interactions (37, 38).

Previous studies have indicated that AnxA2 is asymmetrically distributed in the plasma membrane as a result of its preferential localization to distinct membrane domains rich in phosphatidylinositol 4,5-bisphosphate (39, 40). Because phosphatidylinositol 4,5-bisphosphate-rich regions compose the detergent-insoluble regions of the membrane, AnxA2 has been

identified as a raft-associated protein (41). Although the importance of Ca^{2+} in the localization of AnxA2 to the raft microdomains has been established, it is not known whether localization of AnxA2 to the lipid rafts is influenced by prior signaling events at the membrane. In our studies we observed that disruption of the rafts by MβCD or filipin diminishes the cell surface levels of AnxA2 under elevated levels of intracellular Ca^{2+}. In our experiments filipin was more efficient than MβCD in inhibiting the DRM and cell surface levels of AnxA2. This effect could be due to the release of AnxA2 from cholesterol-rich membranes by filipin as suggested by a previous study (25). It is also known that MβCD does not release AnxA2 from the cholesterol-rich membranes, and hence, the observed effect of MβCD on the cell surface AnxA2 is only a result of the disruption of lipid rafts and not because of the release of AnxA2 from the cholesterol-rich membranes.

Tyr-23 Phosphorylation and Lipid Raft Association of AnxA2—Previous studies have indicated the importance of Ca^{2+} as an indispensable stimulus for the relocation of AnxA2 to the membrane microdomains concentrated in the inner leaflet of the plasma membrane (38, 41–43). Although N-terminal phosphorylation of AnxA2 has been implicated in the regulation of several membrane activities of AnxA2, its involvement in the lipid raft association of AnxA2 has not been previously explored. The present study addressed the role of N-terminal phosphorylation events in the Ca^{2+}-dependent lipid raft localization of AnxA2. Here, we demonstrated that the distribution of AnxA2 to the lipid rafts and also the raft aggregation is markedly influenced by intracellular levels of Ca^{2+}. This translocation is also accompanied by a concomitant increase in the levels of AnxA2 associated with the non-raft regions, suggesting the possibility that AnxA2 binds non-specifically to the non-raft regions of the membrane because of its affinity to the acidic phospholipids and is later recruited to the raft microdomains. Our studies involving both the detergent and non-detergent-based extraction of lipid rafts indicated that only the phosphomimetic mutant at Tyr-23 could be recovered from the lipid rafts. It is well established that proteins recruited to the lipid rafts are phosphorylated in the raft microenvironment by the raft-resident kinases (44). Because the Src kinase Lyn, which is known to phosphorylate AnxA2 at Tyr-23, is localized to the rafts, it is possible that phosphorylation of AnxA2 at Tyr-23 occurs in the kinase-enriched lipid rafts (45). We suggest that phosphorylation at Tyr-23 may impart on AnxA2 the stability of association with the lipid rafts, whereas the non-phosphorylated AnxA2 is destabilized from the raft microdomains.

Lipid Rafts and Protein Sorting—Having demonstrated the involvement of Tyr-23 phosphorylation in the raft recruitment of AnxA2, one of the central questions that would arise subsequently is the role of raft-associated AnxA2. Rafts are originally identified as submicroscopic freely floating assemblies of liquid ordered domains of proteins and lipids (46). The dynamic nature of the rafts enables the movement of both proteins and lipids into and out of the rafts, and rafts are involved in the potentiation of intracellular signaling events (47). Lipid rafts are also known to contribute to membrane trafficking by the formation of transport carriers that form as a result of domain-induced budding from the lipid rafts at the cell surface and the sorting of proteins into a distinct class of endocytic vesicles (28, 48).

Vesicular Sorting of Lipid Raft-associated AnxA2—The internalization of plasma membrane lipid rafts by the intracellular endocytic system has been extensively studied for the transport of glycosylphosphatidylinositol-anchored proteins (31). Endocytosis of protein and lipid raft components can occur via clathrin-dependent and -independent pathways (15). Recent evidence suggests that a majority of the proteins sorted into the lipid raft-internalized vesicles are targeted to early and recycling endosomes via a clathrin-independent pathway (11, 49). In our studies we observed the presence of AnxA2 and CTXB-positive internalized vesicles in the cytosol on ionophore treatment, suggesting that AnxA2 follows similar pathways of lipid raft internalization. Although the mechanisms of lipid raft endocytosis are not known, studies have suggested that proteins and lipids endocytosed via the caveolar pathway are integrated into the classical endosomal system. The budded caveolae referred to as endocytic caveolar carriers have different cellular destinations (50, 51). These vesicles can form a specialized organelle called caveosome in a Rab5-independent manner or can fuse with the endosomes in a RAB5-independent manner (52). Our studies also suggest that AnxA2 is a component of the raft-like microdomains on the late endosomes (data not shown). Although previous studies have suggested that the endosomal rafts are delivered from the plasma membrane by endocytosis via caveolae (53), further studies are essential to establish a direct relation between plasma membrane and endosomal rafts.

Proteins targeted to late endosomes have highly complex sorting systems because of the presence of distinct membrane domains in the late endosomal membranes (54). Sorting of proteins to the late endosomes is a common mechanism for the targeting of proteins to the endoplasmic reticulum and Golgi and transport of certain proteins from the plasma membrane by association with the intralumenal vesicles of the MVEs called exosomes (29). During the process of MVE formation, proteins in the limiting membrane of the early endosomes are targeted to the internal vesicles of the MVE (54).

AnxA2 is known to associate with the endosomal membrane in a Ca^{2+}-independent manner that is different from its Ca^{2+}-dependent interaction with the negatively charged phospholipids (55, 56). The Ca^{2+}-independent interaction of AnxA2 with the vesicular membranes is because of the presence of two copies of the Y*XX*φ (*X* is any other amino acid, and φ is a hydrophobic amino acid) motif in the N terminus of AnxA2 (57). This motif is known to be essential in the interaction of AnxA2 with the clathrin adapter proteins that are involved in the sorting of the cargo to the clathrin-coated vesicles (58). Phosphorylation of AnxA2 at Tyr-23 hinders the interaction of AnxA2 with the clathrin complexes and thereby prevents the endocytosis via clathrin-coated vesicles (58). In the present study we have identified the Ca^{2+}-dependent interaction of AnxA2 with the lipid rafts and its subsequent association with the endosomal system. Our results also indicate that AnxA2 is phosphorylated at Tyr-23 in response to ionophore-induced elevation in intracellular Ca^{2+}. Hence, we suggest that phosphorylation at Tyr-23 hinders the clathrin-dependent endocytosis, and AnxA2 is pos-

sibly endocytosed from the lipid rafts by clathrin-independent endocytosis mediated by caveolae.

Exosomes are internal bilayer vesicles of the MVEs that originate when a limiting membrane of a late endosome is spontaneously invaginated (59). Maturing MVEs that contain several of these internally pinched-off vesicles have three distinct destinations, 1) further maturation to form lysosomes, 2) serve as temporary storage for cellular proteins to avoid a degradation, or 3) secreted as exosomes by the fusion of the MVE limiting membrane with the plasma membrane (60). Biochemical analysis of the secreted exosomal membranes are similar in lipid composition to the rafts, and several raft markers such as GM1, GM3, flotilin, Src kinase, Lyn, and the glycosylphosphatidylinositol-anchored proteins CD55, CD58, and CD59 are known to be associated and secreted by the exosomes (21). These studies suggest that raft-like domains in the late endosomes and MVEs originate as a result of the pinching off of the plasma membrane into intracellular vesicles.

Sorting of AnxA2 from the Plasma Membrane Lipid Rafts to the Exosomes—We demonstrate that ionophore stimulation induces the secretion of exosomes, and exosomal AnxA2 can be exogenously transferred from one cell to another, suggesting the physiological role of exosomes in intercellular communication. The observation that elevated levels of intracellular Ca^{2+} promotes the secretion of exosomes is also supported by previous findings that Ca^{2+} influences multiple membrane fusion events in the trafficking of proteins across the endocytic pathway (61, 62). Furthermore, the isolation of raft-like microdomains from the exosomes has enabled us to determine that AnxA2 is a raft-associated component of the secretory exosomes. We have also studied the exosomal association of Tyr-23 phosphorylation mutants of AnxA2, and our observations demonstrated that the Tyr-23 phosphomimetic mutant of AnxA2 possessed the increased ability to associate with the secretory exosomes, whereas the non-phosphomimetic mutant failed to do so. These observations in addition to our previous findings that prevention of Tyr-23 phosphorylation inhibits the plasma membrane raft association of AnxA2 suggested to us that the raft association of AnxA2 is critical for its entry into the exosomes.

In summary, our data provide insights into several unresolved issues concerning the Ca^{2+}-dependent cell surface translocation of AnxA2. The data presented here suggest several mechanistic approaches that facilitate the sorting of AnxA2 from the raft microdomains of the plasma membrane to the cell surface via its association with the DRMs of the endosomal system. These results outline the importance of secretory exosomes as functional carriers of AnxA2. In conclusion, these observations may suggest an alternate mechanism of non-classical protein secretion.

Acknowledgments—We thank Dr. Michael Oglesby and Sanjay Thamake for editorial assistance, Dr. Jie Liu for providing some of the AnxA2 constructs, and the confocal or transmission electron microscopy core facility for technical assistance.

REFERENCES

1. Gerke, V., Creutz, C. E., and Moss, S. E. (2005) *Nat. Rev. Mol. Cell Biol.* **6,** 449–461
2. Rescher, U., and Gerke, V. (2004) *J. Cell Sci.* **117,** 2631–2639
3. Gerke, V., and Moss, S. E. (2002) *Physiol. Rev.* **82,** 331–371
4. Lambert, O., Cavusoglu, N., Gallay, J., Vincent, M., Rigaud, J. L., Henry, J. P., and Ayala-Sanmartin, J. (2004) *J. Biol. Chem.* **279,** 10872–10882
5. Danielsen, E. M., van Deurs, B., and Hansen, G. H. (2003) *Biochemistry* **42,** 14670–14676
6. Ayala-Sanmartin, J., Zibouche, M., Illien, F., Vincent, M., and Gallay, J. (2008) *Biochim. Biophys. Acta* **1778,** 472–482
7. Rescher, U., Ruhe, D., Ludwig, C., Zobiack, N., and Gerke, V. (2004) *J. Cell Sci.* **117,** 3473–3480
8. Helms, J. B., and Zurzolo, C. (2004) *Traffic* **5,** 247–254
9. Nelson, W. J., and Rodriguez-Boulan, E. (2004) *Nat. Cell Biol.* **6,** 282–284
10. Füllekrug, J., and Simons, K. (2004) *Ann. N.Y. Acad. Sci.* **1014,** 164–169
11. Gagescu, R., Demaurex, N., Parton, R. G., Hunziker, W., Huber, L. A., and Gruenberg, J. (2000) *Mol. Biol. Cell* **11,** 2775–2791
12. Pelkmans, L., Kartenbeck, J., and Helenius, A. (2001) *Nat. Cell Biol.* **3,** 473–483
13. Benlimame, N., Le, P. U., and Nabi, I. R. (1998) *Mol. Biol. Cell* **9,** 1773–1786
14. Nichols, B. J., Kenworthy, A. K., Polishchuk, R. S., Lodge, R., Roberts, T. H., Hirschberg, K., Phair, R. D., and Lippincott-Schwartz, J. (2001) *J. Cell Biol.* **153,** 529–541
15. Sharma, P., Sabharanjak, S., and Mayor, S. (2002) *Semin. Cell Dev. Biol.* **13,** 205–214
16. Hurley, J. H., and Emr, S. D. (2006) *Annu. Rev. Biophys. Biomol. Struct.* **35,** 277–298
17. Wollert, T., and Hurley, J. H. (2010) *Nature* **464,** 864–869
18. Théry, C., Zitvogel, L., and Amigorena, S. (2002) *Nat. Rev. Immunol.* **2,** 569–579
19. Stoorvogel, W., Kleijmeer, M. J., Geuze, H. J., and Raposo, G. (2002) *Traffic* **3,** 321–330
20. Wubbolts, R., Leckie, R. S., Veenhuizen, P. T., Schwarzmann, G., Möbius, W., Hoernschemeyer, J., Slot, J. W., Geuze, H. J., and Stoorvogel, W. (2003) *J. Biol. Chem.* **278,** 10963–10972
21. de Gassart, A., Geminard, C., Fevrier, B., Raposo, G., and Vidal, M. (2003) *Blood* **102,** 4336–4344
22. Abrami, L., Liu, S., Cosson, P., Leppla, S. H., and van der Goot, F. G. (2003) *J. Cell Biol.* **160,** 321–328
23. Bagnat, M., Keränen, S., Shevchenko, A., Shevchenko, A., and Simons, K. (2000) *Proc. Natl. Acad. Sci. U.S.A.* **97,** 3254–3259
24. Beer, C., Andersen, D. S., Rojek, A., and Pedersen, L. (2005) *J. Virol.* **79,** 10776–10787
25. Mayran, N., Parton, R. G., and Gruenberg, J. (2003) *EMBO J.* **22,** 3242–3253
26. Brown, M. T., and Cooper, J. A. (1996) *Biochim. Biophys. Acta* **1287,** 121–149
27. Merendino, A. M., Bucchieri, F., Campanella, C., Marcianò, V., Ribbene, A., David, S., Zummo, G., Burgio, G., Corona, D. F., Conway de Macario, E., Macario, A. J., and Cappello, F. (2010) *PLoS One* 5, e9247
28. Nichols, B. (2003) *J. Cell Sci.* **116,** 4707–4714
29. Sobo, K., Chevallier, J., Parton, R. G., Gruenberg, J., and van der Goot, F. G. (2007) *PLoS One* **2,** e391
30. Savina, A., Vidal, M., and Colombo, M. I. (2002) *J. Cell Sci.* **115,** 2505–2515
31. Parton, R. G., and Richards, A. A. (2003) *Traffic* **4,** 724–738
32. Brown, D. A. (2002) *Curr. Protoc. Immunol.*, Chapter 11, Unit 11.10
33. Silverman, J. M., Clos, J., de'Oliveira, C. C., Shirvani, O., Fang, Y., Wang, C., Foster, L. J., and Reiner, N. E. (2010) *J. Cell Sci.* **123,** 842–852
34. Koga, K., Matsumoto, K., Akiyoshi, T., Kubo, M., Yamanaka, N., Tasaki, A., Nakashima, H., Nakamura, M., Kuroki, S., Tanaka, M., and Katano, M. (2005) *Anticancer Res.* **25,** 3703–3707
35. Zhuang, L., Lin, J., Lu, M. L., Solomon, K. R., and Freeman, M. R. (2002) *Cancer Res.* **62,** 2227–2231
36. Barwise, J. L., and Walker, J. H. (1996) *J. Cell Sci.* **109,** 247–255
37. de Graauw, M., Tijdens, I., Smeets, M. B., Hensbergen, P. J., Deelder, A. M.,

and van de Water, B. (2008) *Mol. Cell. Biol.* **28,** 1029–1040
38. Rescher, U., Ludwig, C., Konietzko, V., Kharitonenkov, A., and Gerke, V. (2008) *J. Cell Sci.* **121,** 2177–2185
39. Hayes, M. J., Shao, D. M., Grieve, A., Levine, T., Bailly, M., and Moss, S. E. (2009) *Biochim. Biophys. Acta* **1793,** 1086–1095
40. Oliferenko, S., Paiha, K., Harder, T., Gerke, V., Schwärzler, C., Schwarz, H., Beug, H., Günthert, U., and Huber, L. A. (1999) *J. Cell Biol.* **146,** 843–854
41. Chasserot-Golaz, S., Vitale, N., Umbrecht-Jenck, E., Knight, D., Gerke, V., and Bader, M. F. (2005) *Mol. Biol. Cell* **16,** 1108–1119
42. Babiychuk, E. B., and Draeger, A. (2000) *J. Cell Biol.* **150,** 1113–1124
43. Deora, A. B., Kreitzer, G., Jacovina, A. T., and Hajjar, K. A. (2004) *J. Biol. Chem.* **279,** 43411–43418
44. Simons, K., and Toomre, D. (2000) *Nat. Rev. Mol. Cell Biol.* **1,** 31–39
45. Arcaro, A., Aubert, M., Espinosa del Hierro, M. E., Khanzada, U. K., Angelidou, S., Tetley, T. D., Bittermann, A. G., Frame, M. C., and Seckl, M. J. (2007) *Cell. Signal.* **19,** 1081–1092
46. Foster, L. J., and Chan, Q. W. (2007) *Subcell. Biochem.* **43,** 35–47
47. Rajendran, L., and Simons, K. (2005) *J. Cell Sci.* **118,** 1099–1102
48. Schuck, S., and Simons, K. (2004) *J. Cell Sci.* **117,** 5955–5964
49. Le Roy, C., and Wrana, J. L. (2005) *Nat. Rev. Mol. Cell Biol.* **6,** 112–126
50. Pfeffer, S. R. (2001) *Nat. Cell Biol.* **3,** E108–110
51. Pelkmans, L., Bürli, T., Zerial, M., and Helenius, A. (2004) *Cell* **118,** 767–780
52. Parton, R. G. (2004) *Dev. Cell* **7,** 458–460
53. Simons, K., and Gruenberg, J. (2000) *Trends Cell Biol.* **10,** 459–462
54. Gruenberg, J., and Stenmark, H. (2004) *Nat. Rev. Mol. Cell Biol.* **5,** 317–323
55. Morel, E., Parton, R. G., and Gruenberg, J. (2009) *Dev. Cell.* **16,** 445–457
56. Zeuschner, D., Stoorvogel, W., and Gerke, V. (2001) *Eur. J. Cell Biol.* **80,** 499–507
57. Turpin, E., Russo-Marie, F., Dubois, T., de Paillerets, C., Alfsen, A., and Bomsel, M. (1998) *Biochim. Biophys. Acta* **1402,** 115–130
58. Creutz, C. E., and Snyder, S. L. (2005) *Biochemistry* **44,** 13795–13806
59. Booth, A. M., Fang, Y., Fallon, J. K., Yang, J. M., Hildreth, J. E., and Gould, S. J. (2006) *J. Cell Biol.* **172,** 923–935
60. Simons, M., and Raposo, G. (2009) *Curr. Opin. Cell Biol.* **21,** 575–581
61. MacDonald, P. E., Eliasson, L., and Rorsman, P. (2005) *J. Cell Sci.* **118,** 5911–5920
62. Mayorga, L. S., Berón, W., Sarrouf, M. N., Colombo, M. I., Creutz, C., and Stahl, P. D. (1994) *J. Biol. Chem.* **269,** 30927–30934
63. Rubin, D., and Ismail-Beigi, F. (2003) *Am. J. Physiol. Cell Physiol.* **285,** C377–383
64. Savina, A., Furlán, M., Vidal, M., and Colombo, M. I. (2003) *J. Biol. Chem.* **278,** 20083–20090